US 20090180887A1

(19) **United States**

(12) **Patent Application Publication**

(10) **Pub. No.: US 2009/0180887 A1**

(43) **Pub. Date: Jul. 16, 2009**

Mischo et al.

(54) **TURBINE BLADE WITH RECESSED TIP**

(76) Inventors: **Bob Mischo**, Zürich (CH); **Reza Abhari**, Forch (CH); **Thomas Behr**, Zurich (CH)

Correspondence Address:
PAULEY PETERSEN & ERICKSON
2800 WEST HIGGINS ROAD, SUITE 365
HOFFMAN ESTATES, IL 60169 (US)

(21) Appl. No.: **12/087,761**

(22) PCT Filed: **Jan. 15, 2007**

(86) PCT No.: **PCT/EP2007/050336**

§ 371 (c)(1),
(2), (4) Date: **Nov. 14, 2008**

Related U.S. Application Data

(60) Provisional application No. 60/758,763, filed on Jan. 13, 2006.

Publication Classification

(51) **Int. Cl.**
F01D 5/14 (2006.01)

(52) **U.S. Cl.** ..... **416/223 R**

(57) **ABSTRACT**

A turbine blade (**1**) with a side surface (**7**) having an aerodynamic profile. The turbine blade (**1**) further comprises an end surface (**6**) and is mounted in a turbine, whereby the end surface (**6**) is delimited by a gap from a casing (**8**) of the turbine. The end surface (**6**) comprises a recess (**2**) which is shaped such that it acts as an improved aerodynamic seal.

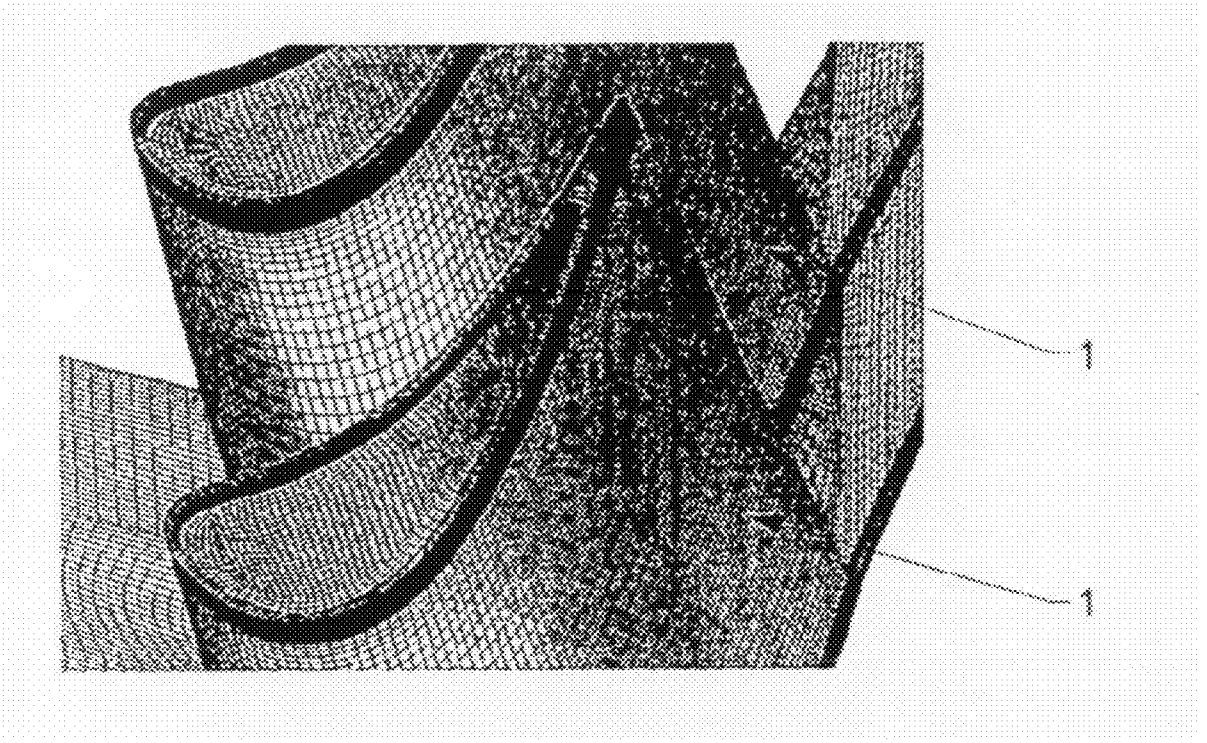

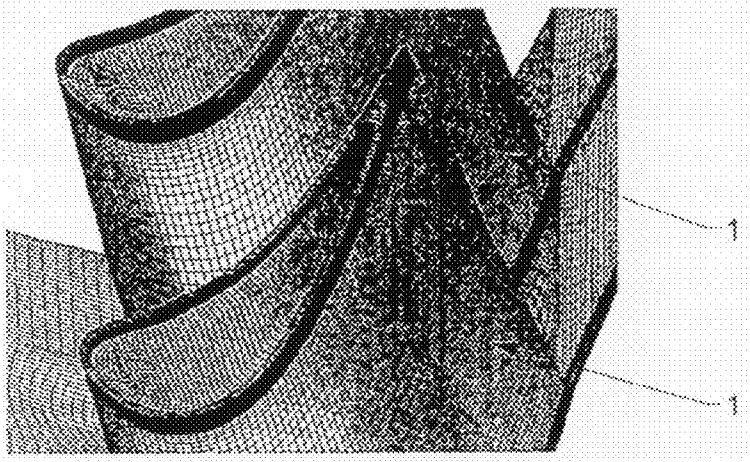

Fig. 1

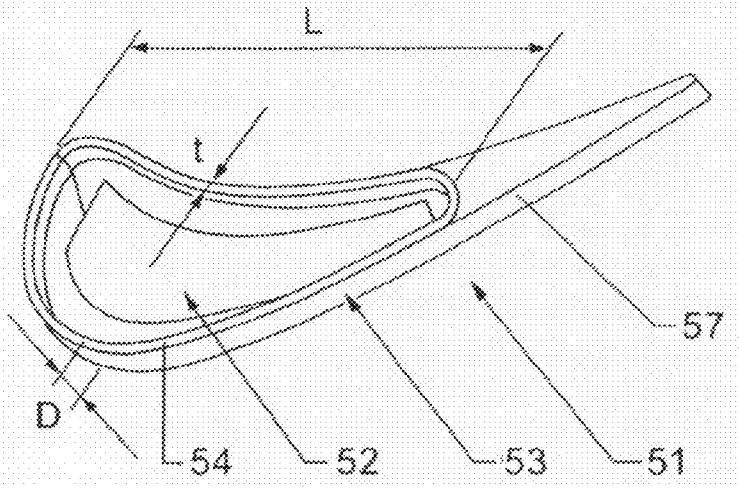

Fig. 2

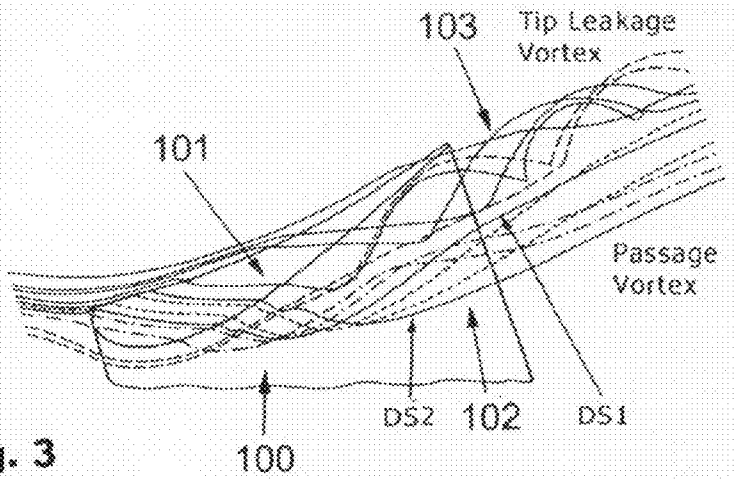

Fig. 3

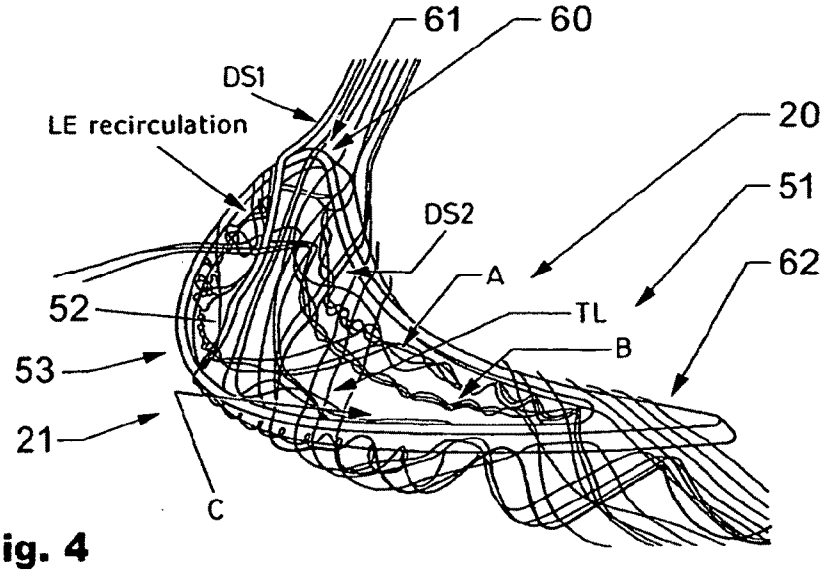

Fig. 4

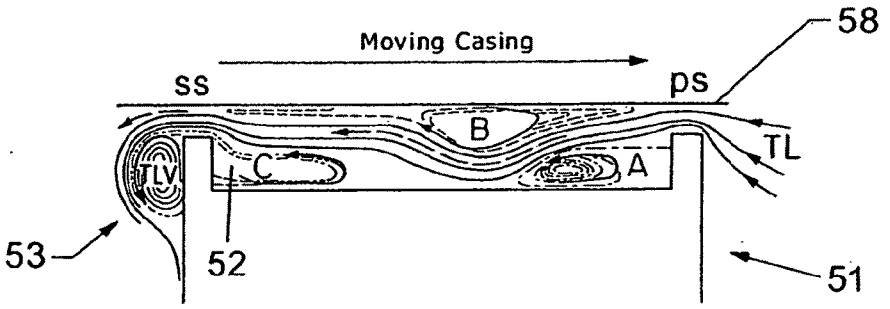

Fig. 5

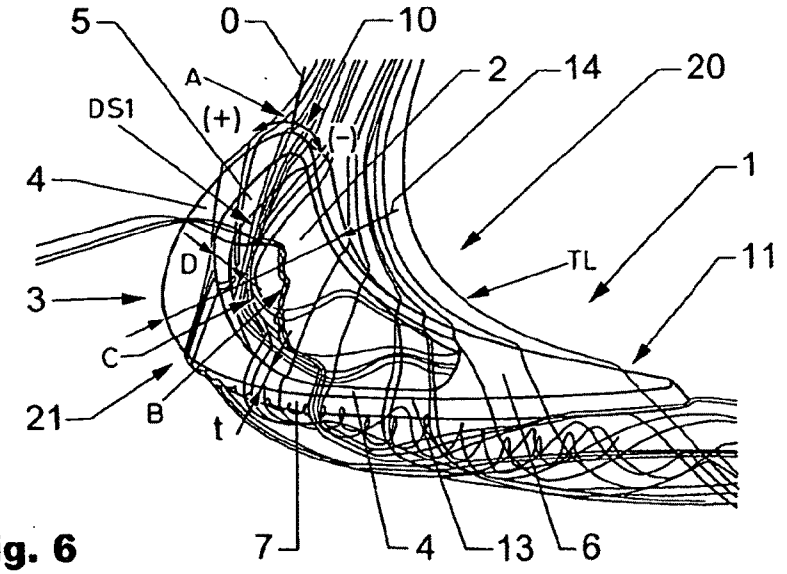

Fig. 6

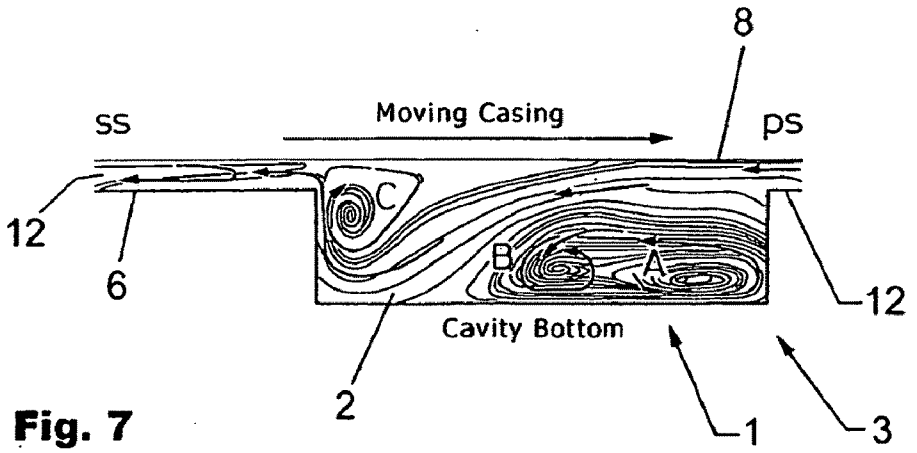

Fig. 7

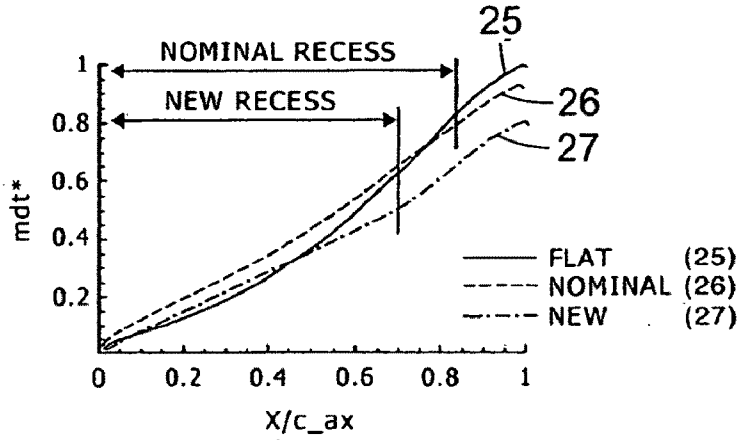

Fig. 8

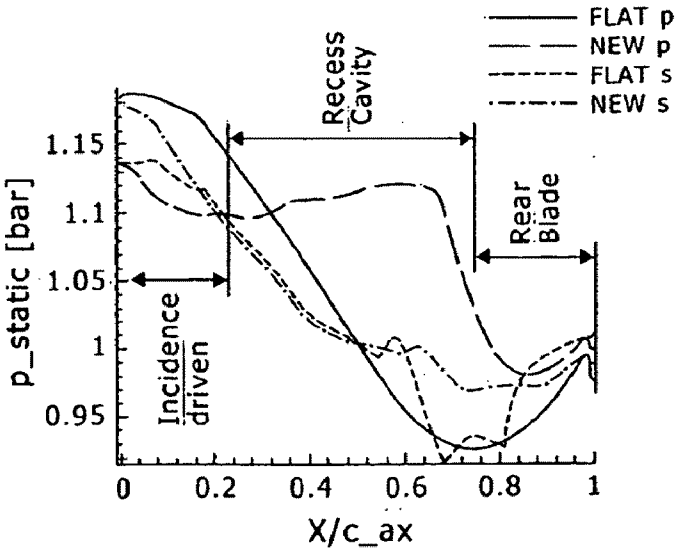

Fig. 9

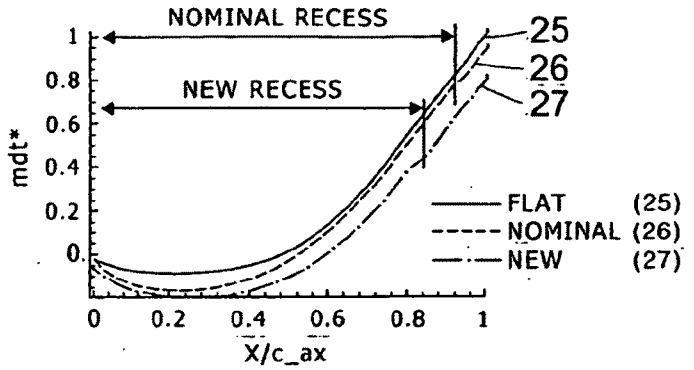

Fig. 10

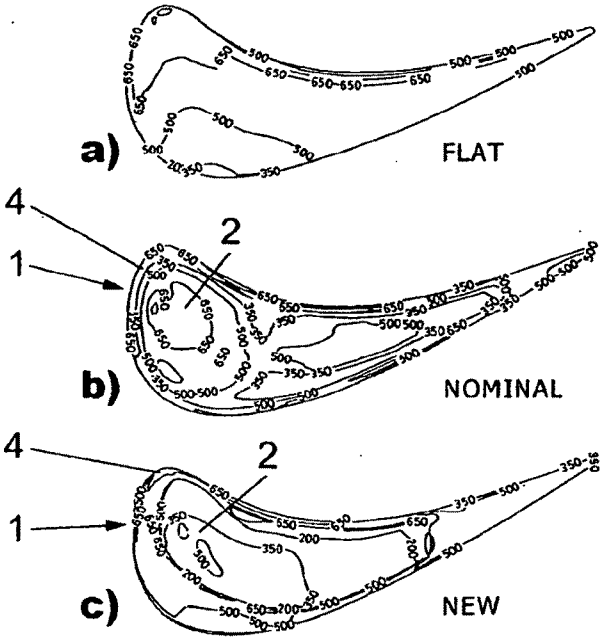

Fig. 11

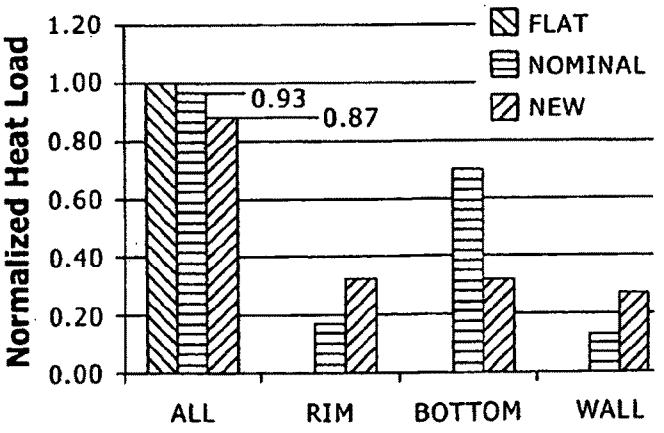

Fig. 12

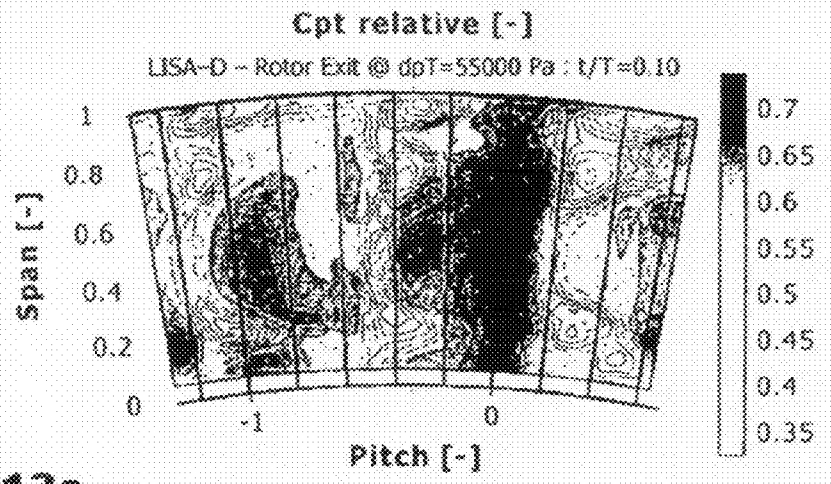

Fig. 13a

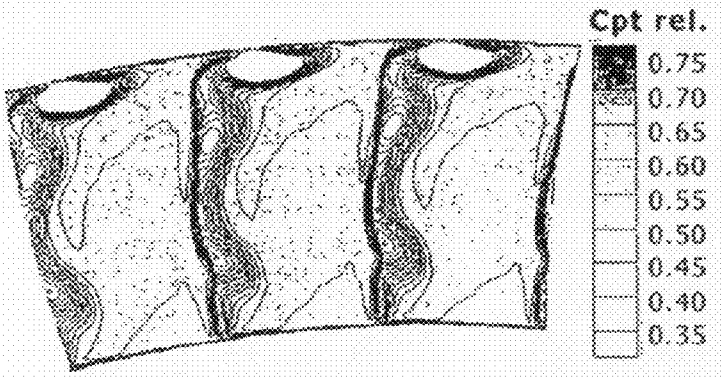

Fig. 13b

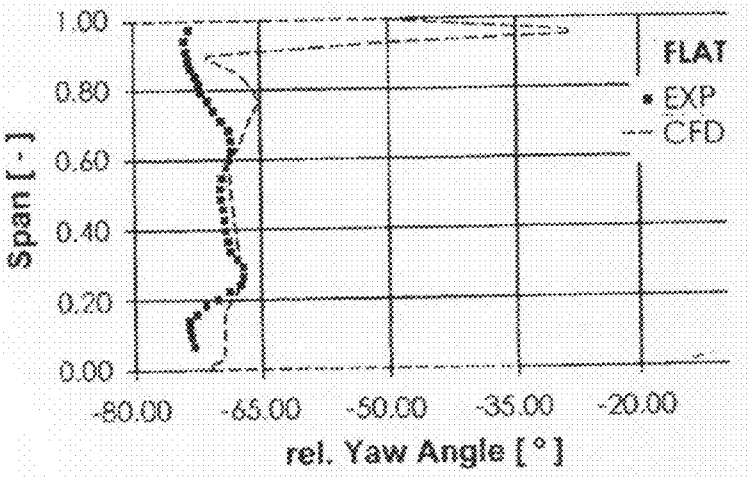

Fig. 13c

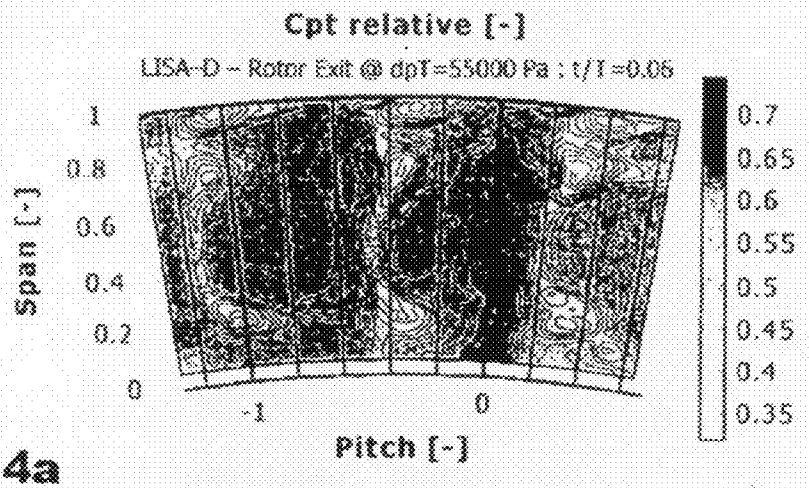

Fig. 14a

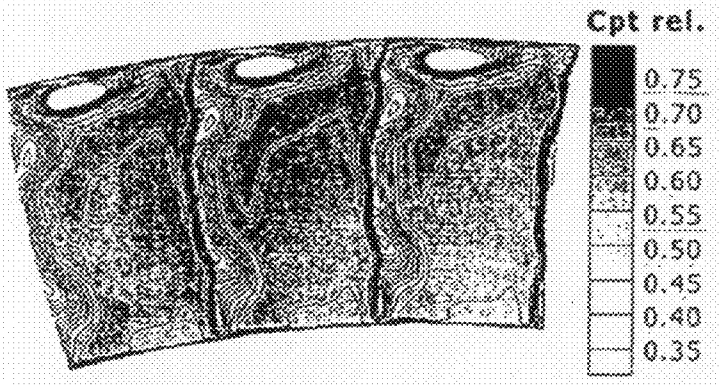

Fig. 14b

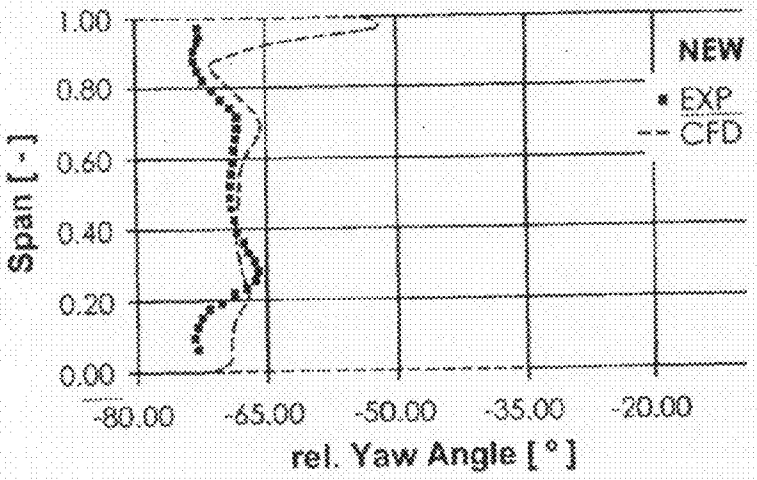

Fig. 14c

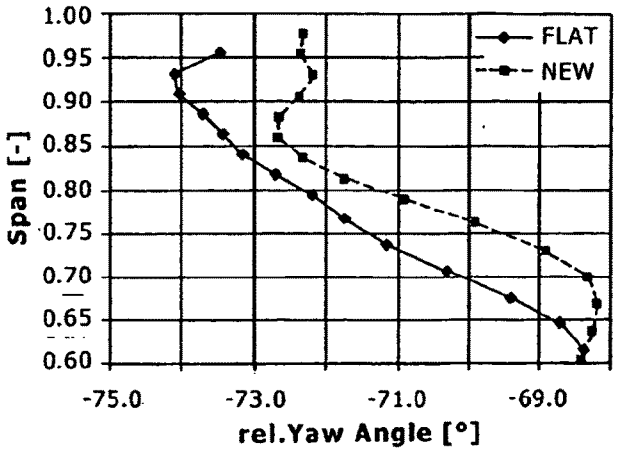

Fig. 15

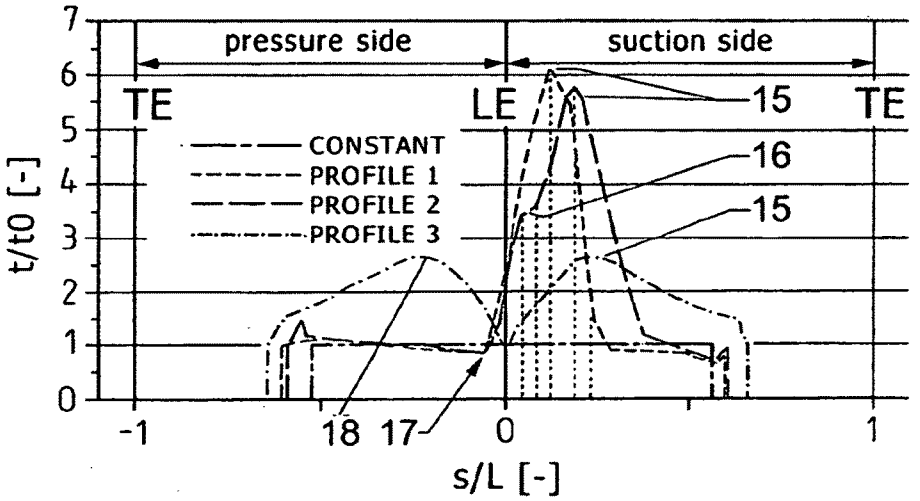

Fig. 16

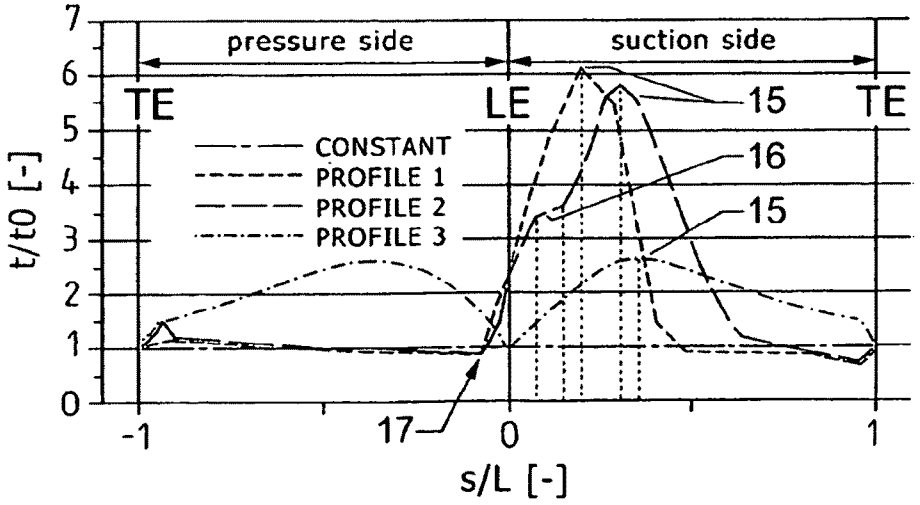

Fig. 17

TURBINE BLADE WITH RECESSED TIP

FIELD OF THE INVENTION

[0001] The invention lays in the field of turbine blades for highly loaded axial rotor turbines as e.g. used in aero engines or for power generation.

DESCRIPTION OF THE ART

[0002] In axial turbine the tip clearance flow occurring in rotor blade rows is responsible for about one third of the aerodynamic losses in the blade row and in many cases is the limiting factor for the blade lifetime.

[0003] The tip leakage vortex forms when the leaking fluid crosses the gap between the rotor blade tip and the casing from pressure to suction side and rolls up into a vortex on the blade suction side. The flow through the tip gap is both of high velocity and high temperature, with the heat transfer to the blade from the hot fluid being very high in the blade tip area. In order to avoid blade tip burnout and a failure of the machine, blade tip cooling is commonly used.

[0004] The tip clearance flow has been investigated recently with a number of contributions in the open literature. An important contribution always referred to is the work by Rains [1] (see subsequent list of references), who studied tip clearance flow for axial flow pump motivated by concerns of cavitation. Moore & Tilton [2] investigate the tip leakage flow both experimentally and analytically. The flow structure inside the gap and heat transfer to the blade have been discussed. A flow model assuming the gap losses coming from complete mixing behind the vena contracta (in general, point in a fluid stream where the diameter of the stream is the least) leading to uniform flow conditions at the gap outlet is presented. Bindon [3] measured and investigated the tip clearance loss formation. He could divide the total endwall loss into loss generated inside the tip gap, mixing loss of the tip leakage vortex, and secondary and endwall losses. He concluded that not only tip leakage mass flow is important for loss generation (48% of overall loss seen in mixing loss), but also the flow structure inside the gap would play a significant role (39% of overall loss generated inside the gap). Furthermore, he showed a conceptual model for tip clearance loss formation. Bindon & Morphis [4] investigated loss for different blade tip geometries. They found that the overall loss remained unchanged although gap losses strongly varied between the base line sharp edged flat tip and differently contoured blade tips. Whereas the sharp edge case showed high losses inside the gap with a strong separation bubble at the pressure side lip, the contoured cases showed less losses since no separation bubble was formed on the gap inlet but in turn an increased tip gap mass flow was found.

[0005] In a study of different squealer tips by Heyes, Hodson & Dailey [5] it was also concluded that the separation bubble with the associated vena contracta is effectively sealing the gap and by reducing tip mass flow the tip clearance losses may be decreased. In this study also a flow model for squealer tips is included as well as a model for the flow at the gap exit which is represented as a combination of an isentropic jet between the casing and gap mid height and a wake formed behind the separation bubble. A computational study by Ameri [6] on heat transfer on the blade tip showed that a flat tip with sharp edges performs best in terms of efficiency and total pressure loss compared to a mean camberline squealer tip and a flat tip with radiused blade tips. Further computational studies by Tallman [7], [8] on the experimentally investigated linear cascade by Bindon & Morphis [4] discuss the effect of tip clearance height and relative casing wall movement on the flow physics in the tip gap. A further experimental investigation on the tip clearance flow physics due to moving casing wall is presented in a two part study by Yaras & Sjolander [9,10]. It was found that the moving belt simulating relative casing motion significantly decreased tip gap mass flow. Also the tip passage vortex is drawn to the suction side, providing a throttling effect. Furthermore a reduced pressure difference driving the flow into the gap was observed.

[0006] In a recent study, detailed heat transfer to recessed blade tip was first investigated by Dunn et al. [12]. A recessed blade tip was equipped with heat flux gauges and experimentally investigated in a full stage rotating turbine. Nusselt Number was shown for different vane/blade spacings. It was found that the leading edge Nusselt Number on the cavity bottom were in excess of the blade stagnation value.

LIST OF REFERENCES

[0007] [1] Rains, D. A., 1954, "Tip Clearance Flows in Axial Flow Compressors and Pumps", California Institute of Technology, Hydrodynamics and Mechanical Engineering Laboratories, Report No. 5, June 1954.

[0008] [2] Moore, J. & Tilton, J. S., 1988, "Tip Leakage Flow in a Linear Turbine Cascade,", ASME Journal of Turbomachinery, Vol 110, pp. 18-26.

[0009] [3] Bindon, J. P., 1989, "The Measurement and Foramtion of Tip Leakage Loss," ASME Journal of Turbomachinery, Vol 111, pp. 257-263.

[0010] [4] Morphis, G. & Bindon, J. P., 1992, "The Development of Axial Turbine Leakage Loss for Two Profiled Tip Geometries Using Linear Cascade Data," ASME Journal of Turbomachinery, Vol 114, pp. 198-203.

[0011] [5] Heyes, F. J. G., Hodson, H. P., & Dailey, G. M., 1992, "The Effect of Blade Tip Geometry on the Tip Leakage Flow in Axial Turbine Cascades," ASME Journal of Turbomachinery, Vol 114, pp. 643-651.

[0012] [6] Ameri Ali, A., 2001, "Heat Transfer and Flow on the Blade Tip of a Gas Turbine Equipped with a Mean-Camberline Strip," ASME Paper 2001-GT-0156.

[0013] [7] Tallman, J. & Lakshminarayana B., 2000, "Numerical Simulation of Tip Clearance Flows in Axial Flow Turbines, With Emphasis on Flow Physics, Part I—Effect of Tip Clearance Height," ASME Journal of Turbomachinery, Vol 123, pp. 314-323.

[0014] [8] Tallman, J. & Lakshminarayana B., 2000, "Numerical Simulation of Tip Clearance Flows in Axial Flow Turbines, With Emphasis on Flow Physics, Part II—Effect of Outer Casing Relative Motion," ASME Journal of Turbomachinery, Vol 123, pp. 324-333.

[0015] [9] Yaras, M. I. & Sjolander, S. A., 1992, "Effects of Simulated Rotation on Tip Leakage in a Planar Cascade of Turbine Blades: Part I—Tip Gap Flow," ASME Journal of Turbomachinery, Vol 114, pp. 652-659.

[0016] [10] Yaras, M. I. & Sjolander, S. A., 1992, "Effects of Simulated Rotation on Tip Leakage in a Planar Cascade of Turbine Blades: Part II—Downstream Flow Field and Blade Loading," ASME Journal of Turbomachinery, Vol 114, pp. 660-667.

[0017] [11] Basson, A. H. & Lakshminarayana, B., 1995, "Numerical Simulation of Tip Clearance Effects in Turbomachinery," ASME Journal of Turbomachinery, Vol 109, pp. 545-549.

[0018] [12] Dunn, M. G. & Haldemann, C. W., 2000, "Time Averaged Heat Flux for a Recessed Blade Tip, Lip and Platform of a Transonic Turbine Blade", ASME Paper GT2000-0197.

[0019] [13] Behr, T., Kalfas, A. I., Abhari, R. S., "Unsteady Aerodynamics in Casing Injection for Tip Leakage Treatment in an Oneand-½-Stage Unshrouded Turbine", ASME Paper No. GT2006-90959.

[0020] [14] Sell M., Schlienger J., Pfau A., Treiber M., Abhari R. S., 2001, "The 2-stage Axial Turbine Test Facility LISA", ASME Paper No. 2001-GT-049.

SUMMARY OF THE INVENTION

[0021] The invention is directed to a recessed blade tip for a highly loaded axial rotor turbine blade with application in high pressure axial turbines in aero engine or power generation.

[0022] To overcome the problems known from the prior art a blade tip design is suggested with a recess in the blade tip instead of a simple flat blade tip. The recess (cavity) inside the blade tip acts as an aerodynamic seal which improves the performance of the turbine and/or reduces the heat load of the turbine tip, in that it takes influence on the flows distribution. Since material at the upper surface of the blade is moved to a lower radius from the axis of is rotation, blade root mechanical stresses can be lowered. Also in case of a tip rub, i.e. when the rotor blade touches the casing during rotation, only the thin cavity rim is damaged. Wear damage to the casing is also limited and since the purge holes for the blade tip cooling are located inside the cavity, the rubbing does not damage the outlet of the holes. Efficient cooling is hence assured even if rubbing occurs. Finally, the recess cavity may act as a labyrinth seal, which could be beneficial in reducing tip clearance mass flow.

[0023] It has been observed that by an appropriate profiling of the recess shape, the total tip heat transfer Nusselt Number can significantly reduced, e.g. being 15% lower than the flat tip and 7% lower than the baseline recess shape. Experimental results also showed an overall improvement of 0.3% in the overall turbine total efficiency with the improved recess deign compared to the flat tip case, validating a 0.38% prediction from the CFD analysis.

[0024] With use of a three dimensional Computational Fluid Dynamics (CFD), the flow field near the tip of the blade for different shapes of the recess cavities is investigated. Through control of cavity vertical structures, an improved design is achieved and the differences to the blade tips as common in prior art are highlighted.

[0025] Tip clearance between the blade tip of a rotor and the casing is necessary for a free rotation of the rotor blade row. The gap however allows fluid to cross the blade tip from the pressure side of the blade to the suction side due to the pressure difference on the pressure and the suction side. This flow is associated with two main problems. Firstly, roughly one third of all the aerodynamical losses in a rotor row are related to the tip leakage vortex, which forms when the tip leakage over the blade tip enters the passage flow again on the blade suction side. It creates both mixing loss when it mixes out with the main flow and perturbs the pressure field on the blade tip wall that is responsible for the blade lift. Furthermore, the fluid crossing the gap is not turned by the blade and therefore no work is extracted from it. It is therefore interpreted as lost work extraction. Secondly, the fluid crossing the tip clearance has a relatively high temperature due to hot streak migration, resulting in a high thermal load for the blade tip. In fact, blade tips burn away if not adequately cooled and are hence one of the limiting factor for the blade lifetime.

[0026] Additionally, it is desirable to minimize the tip clearance gap height in order to improve the performance through reduction of the tip leakage mass flow. This reduced gap height, however, increases the risk of the rotor blade rubbing at the casing sometime during the operational envelope. This can occur for example if the rotor expands further than the casing due to transients, a rotor dynamic excursion, an ovalization of the casing, or through casing thermal distortions. In the case that a blade with a flat tip rubs severely at the casing, catastrophic coolant loss could occur if the tip wears off. Even in a case of a relatively minor rub for a flat tip, any cooling holes located on the tip may be damaged resulting in an inadequate cooling eventually leading to blade tip burnout.

[0027] Unlike for the case of a flat blade tips, the more complex flow physics for a recessed blade tip is more difficult to understand it's complexity. Also systematic design procedures for cavity size and shape are not available. By research it was possible to overcome this problem and to better understand aerodynamics and heat transfer physics of recess cavities and to provide new design boundaries for a standard, highly loaded rotor blade representative of a high pressure turbine. A special three dimensional CFD tool has been extensively used for this purpose.

Nomenclature

[0028]

Cartesian coordinates	X (axial), Y, Z
Cylindrical coordinates	R(radial), θ, X
Blade axial chord	$c_{ax} = X_{LE\ blade} - X_{LE\ blade}$
Tip clearance height	$h = \frac{R_{Blade\ Tip} - R_{Hub}}{R_{Hub} - R_{Casing}}$
Recess length	L
Recess depth	D
Recess rim thickness	$t(L, D)$
Static pressure	p_s
Relative Total pressure	p_{tr}
Mass Flow	$\dot{m} = \int_A \vec{c} \cdot d\vec{A}$
Normalized quantity to flat tip	$Q^* = \frac{Q}{Q_{FLAT\ TIP}}$
Total pressure Loss coefficient	$Cpt = \frac{p_{tr\ in} - p_{tr\ out}}{p_{tr\ out} - p_{s\ out}}$
Efficiency	$\eta_m = \frac{\left(\frac{\omega \cdot M}{\dot{m}}\right)}{\left(c_p T_{in}\left(1 - \left(\frac{p_{t,out}}{p_{t,in}}\right)^{\frac{\kappa-1}{\kappa}}\right)\right)}$

[0029] The invention as such and computational tools to improve the results are described in general in accordance with the drawings. Because not available on the marked the computational tools for pre-processing and the solver have been developed by the inventors. These tools may interact in parts with commercial products for post-processing.

[0030] In order to perform the intended computational and experimental study, a previously designed axial turbine test case has been utilized. The geometry of the one-and-½-stage, unshrouded turbine models a highly loaded (DH/U^2=2.36), low aspect ratio gas turbine environment. The air-loop of the test rig is of a quasi-closed type and includes a radial compressor, a two-stage water to air heat exchanger and a calibrated venturi nozzle for mass flow measurements. Before the flow enters the turbine section, it passes through a 3 Meter long straight duct, which contains flow straighteners to ensure an evenly distributed inlet is, flow field. Downstream of the turbine the air-loop is open to atmospheric conditions. A DC generator absorbs the turbine power and controls the rotational speed of the turbine. An accurate torque meter measures the torque that is transmitted by the rotor shaft to the generator. The TET (turbine entry temperature) is controlled to an accuracy of 0.3% and the RPM (Rounds Per Minute) is kept constant within ±0.5 min^{-1} by the DC generator. More information on the turbine design (Behr et al. [13]) as well as on the operation of the experimental facility (Sell et al. [14]) can be found in the open literature.

[0031] The following table shows the main parameter of "LISA" 1.5-stages axial turbine research facility at design operating point (Table 1):

Turbine	
Rotor speed [RPM]	2700
Pressure ratio (1.5-Stage, total-to-static)	1.60
Turbine entry temperature (TET) [° C.]	55
Total inlet pressure [bar abs norm]	1.4
Mass flow [kg/s]	12.13
Shaft Power [kW]	292
Hub/Tip Diameter [mm]	660/800
1st Stage	
Pressure ratio (1st Stage, total-to-total)	1.35
Degree of reaction [−]	0.39
Loading coefficient y = Dh/u2 [−]	2.36
Flow coefficient f = cx/u [−]	0.65

[0032] A computational design optimization for a nominal recess cavity commonly used in axial turbine rotor blades has been presented. From extensive parametric study, an improved recess cavity design is presented. Extensive aerodynamic and heat transfer comparisons between the new design and the flat tip blade and the nominal recess tip are presented. The computational data was compared to experimental data of the Swiss Federal Institute of Technology (ETHZ) where the 3D flow structures and the performance of rotor blades with flat tip and the new recess design were measured. Qualitative comparisons to the experimental data from OSU have also been used to validate the predicted heat transfer data. The following concluding statements can be drawn from this study.

[0033] A better understanding of the three dimensional flow inside recess cavities was gained. Three cavity vortices were found to govern the leakage flow through the cavity.

[0034] Change of the cavity geometry influences the generation and the interaction of the main recess vortices. A particular recirculation at the suction side front responsible for high heat transfer could be eliminated and lead to a new design with improved heat transfer behaviour.

[0035] The beneficial effect of creating an aerodynamic seal has been shown for both recess designs. Tip leakage mass flow could be lowered by as much as 25% in the new recess design according to the present invention compared to the flat tip. CFD showed increased power output for the new design too. Experimental measurements showed a 0.3% increase in the turbine efficiency between a flat tip and the new recess tip at design point.

[0036] The heat load on the blade tip is found to be a balance between the heat load on the different blade tip components, i.e. the tip rim, the cavity rim walls, the cavity bottom and the rear flat blade tip. The new recessed design is about 7% lower on the overall heat load compared to the base line recessed design and 15% lower compared to the flat tip.

[0037] To the best of the author's knowledge, this is the first time that detailed profiling of blade tip recess cavity is shown to improve performance and reduce heat load.

[0038] Three-dimensional geometric profiling of blade tip recess cavity walls significantly improves overall efficiency and effectively reduces in the same time both heat load at the blade tip and mechanical stress.

[0039] Three-dimensional geometric profiling of recess cavity walls can be achieved by using non-uniform rim wall thickness as well as three-dimensional shaping of the inside of the cavity recess volume.

[0040] Three-dimensional geometric profiling occurs through varying the recess rim thickness and cavity depth either separately or combine.

[0041] Three-dimensional geometric profiling of recess cavity optimize leakage flow and its interaction with vortices within the cavity and suppresses vertical flow formation leading to loss in the cavity through flow and high heat load on the cavity walls.

[0042] Three-dimensional geometric profiling of blade tip recess cavities showing the above features attenuates and suppresses the secondary vortex formation and by restraining the available space required for vortex formation both circumferentially and radially.

[0043] Three-dimensional profiling of recess cavity walls leads to higher work output of the blade because of additional blade surface of the cavity walls in case of a favourable cavity pressure gradient.

[0044] Three-dimensional geometric profiling according to the above features define an optimum cavity volume to combine.

[0045] Three-dimensional geometric profiling exhibiting the above features reduces the number of circumferentially aligned vortices.

[0046] Three-dimensional geometric profiling exhibiting the above features leads to less dissipative vortex patterns inside the cavity.

[0047] Three-dimensional geometric profiling of blade tip recess cavities showing the above features keeps the advantages of non-profiled, constant rim thickness cavities, such as reduced rubbing surface area, cooling hole protection, lower mechanical stresses.

[0048] Three-dimensional geometric profiling of blade tip recess cavities showing the above features is applicable for unshrouded and certain partially shrouded turbine blades.

[0049] Three-dimensional geometrically profiled tip recess cavity walls showing the above features provide passive flow control of leakage flow by acting as a throttling mechanism.

[0050] Three-dimensional geometrically profiled tip recess cavity walls based on the three-dimensional flow structure showing the above features can be used to re-design the blade tips of both existing blades for the upgrade and replacement blades as well as being incorporated into new design configurations.

[0051] The invention is directed to a turbine blade with a side surface having an aerodynamic profile. The turbine blade has an end surface arranged in a mounted position in a turbine delimited by a gap from a casing of the turbine. The end surface comprises a recess which is shaped such that it acts as an aerodynamic seal and/or reduces the blade tip heat load. The recess is delimited by a side wall which has a variable wall thickness in circumferential direction. The side wall may have an in general constant wall thickness in height direction (in the direction of the length of the turbine blade). In certain embodiments the wall thickness of the side wall has an overall maximum in the area where the turbine blade has its maximum thickness. In a further embodiment the wall thickness of the side wall has a maximum on the suction side of the turbine blade between +0% and +50% relative length with respect to the blade leading edge (trailing edge +/−100%). In certain embodiments this maximum is an overall maximum. However, in certain other embodiments the wall thickness of the side wall has on the pressure side of the turbine blade a minima. Depending on the field of application this may be located in the range between −0% and −70% relative length with respect to the blade leading edge stagnation point (0%). The wall thickness on the pressure side may be at least partially constant. Good results may be achieved in that the overall maximum of the wall thickness of the side wall is about 5.5 to 6.5 times bigger then the overall minima. In an embodiment the recess has an in general constant depth.

BRIEF DESCRIPTION OF THE DRAWINGS

[0052] The herein described invention will be more fully understood from the detailed description given herein below and the accompanying drawings which should not be considered limiting to the invention described in the appended claims. The drawings show in a simplified and schematic manner

[0053] FIG. **1** an example of a three dimensional computational grid turbine rotor blade with a recess cavity;

[0054] FIG. **2** an example of a recess cavity design according to the prior art;

[0055] FIG. **3** a three dimensional CFD flow distribution over flat tip blade as known from the prior art;

[0056] FIG. **4** a three dimensional CFD flow distribution around a first embodiment of a tip with a recess according to the prior art;

[0057] FIG. **5** a two dimensional CFD flow distribution in the recess according to FIG. **4**;

[0058] FIG. **6** a three dimensional flow distribution around a blade tip with a recess according to the invention;

[0059] FIG. **7** the flow distribution according to FIG. **6** in a cut view;

[0060] FIG. **8** a pressure side CFD normalized tip mass flow;

[0061] FIG. **9** CFD Predicted Tip Rim Static;

[0062] FIG. **10** Suction Side CFD Predicted Normalized Tip Mass Flow;

[0063] FIG. **11** CFD Blade Tip Nusselt Number Distribution;

[0064] FIG. **12** CFD Predicted Normalized Heat Load for Flat Tip, Nominal Recess and New Recess;

[0065] FIG. **13***a* Experimental Relative Total Pressure Coefficient Distribution at 14% axial chord downstream Rotor Blade Trailing Edge For Flat Tip Blade;

[0066] FIG. **13***b* CFD Predicted Relative Total Pressure Coefficient Distribution at 14% axial chord downstream Rotor Blade Trailing Edge, Flat Tip Blade;

[0067] FIG. **13***c* Steady CFD Prediction vs pitch averaged Experimental Relative Yaw Angle at 14% axial chord downstream Rotor Blade Trailing Edge, Flat Tip Blade;

[0068] FIG. **14***a* Experimental Relative Total Pressure Coefficient Distribution at 14% axial chord downstream Rotor Blade Trailing Edge, New Recess Tip Blade;

[0069] FIG. **14***b* CFD Predicted Relative Total Pressure Coefficient Distribution at 14% downstream Rotor Blade Trailing Edge For New Recess Tip Blade;

[0070] FIG. **14***c* CFD Predicted vs Experimental pitch averaged Relative Yaw Angle at 14% axial chord downstream Rotor Blade Trailing Edge For New Recess Tip Blade;

[0071] FIG. **15** experimental pitch averaged relative yaw angle at 14% axial chord downstream rotor blade trailing edge for new recess tip blade

[0072] FIG. **16** shows a first graph of a wall thickness distribution of a recess in a turbine tip;

[0073] FIG. **17** shows a second graph of a wall thickness distribution of a recess in a turbine tip.

DESCRIPTION OF THE EMBODIMENTS

[0074] Subsequent embodiments of the invention are described in more detail. Similar features are in the different drawings marked with the same numbers.

[0075] FIG. **1** shows a computer model of two turbine blades for numerical calculation of the behaviour of a recess arranged at the tip of a turbine blade.

[0076] The analytical models applied are in general based on a numerical grid (mesh) of a turbine blade **1**. The numerical grids used were generated with an in-house developed grid generator called MELLIP. A multi block structured grid generator uses a two dimensional NURBS library as input data to mesh the computational domain boundaries. Using a set of geometrical transformations the interior block boundaries are defined according to the intended grid topology. High grid quality, i.e. smooth gridlines, limited aspect ratio, skewness and cell to cell ratios are achieved using both non linear interpolation algorithms with flexible clustering specification and two dimensional Poisson type elliptic partial differential equations during the meshing of each block. Several topologies are implemented and partition the computational domain for a blade tip with recess area in 18 blocks for the blade recess case. Especially the use of up- and downstream wake blocks with adjustable sizes and grid density helps to keep low grid skewness in the trailing edge area and prevents the numerical diffusion of the shed wake. The grids used for this study show a high resolution in the blade tip area in order to capture the flow gradients in this region.

[0077] This helps in keeping the number of grid points at about 900'000 points, since clustering near walls does not need to be as aggressive as in two layer turbulence model computations. Hence the high number of grid points in the blade tip area leads to homogeneous mesh density with smooth cell to cell ratios distribution. The densely packed tip region grid block spans over about the top 10% the blade span.

[0078] A numerical flow solver preferably used is called MBStage3D, a three-dimensional, structured Navier-Stokes solver for multistage turbomachinery applications. The time marching algorithm preferably used in MBStage3D is a Jameson-type algorithm, i.e. an explicit method with a residual-averaging technique applied for improving stability. The time discretization is preferably accomplished by a five stage Runge-Kutta technique, which is of fourth-order accuracy. All computations discussed here were conducted with the algebraic Baldwin-Lomax turbulence model together with the Sommerfeld logarithmic wall function to compute the turbulent viscosity at the wall.

[0079] Extensive post processing necessary to gain understanding of flow physics is achieved through 3D, 2D, 1D, and scalar investigation of the flow fields of interest. The 3D visualizing is done with TECPLOT, a collection of integrators and the 3D data generation subroutines for TECPLOT are developed in-house.

[0080] FIG. **2** schematically shows a common turbine blade **51** as known from the prior art. The Turbine blade **51** has an outer side surface **57** with an aerodynamic profile. It further comprises an end surface **56** which is in a mounted position in a turbine arranged at a distance to a casing **58** of the turbine (see FIG. **5**). The end surface **56** comprises a recess **52** which is shaped such that it acts as an aerodynamic seal. The recess **52** at the blade tip **53** has a length L and a uniform depth D. The wall **54** surrounding the recess **2** has a constant thickness t in vertical and circumferential direction. An investigation of the three dimensional flow-field around the blade tip **53** and the recess **52** having a length L of 80% of the axial chord (depth of wing) and a depth D of twice the tip gap height allowed to identify the flow features in an exemplary manner.

[0081] The geometry of the tip recess **52** and its impact on the distribution of the flow field around the blade tip **53** was investigated based on a standard (nominal) recess design **52** (see FIGS. **2**, **4**, **5**) to find further improved recess designs. The main geometrical parameters varied were the length L of the recess cavity, the depth D of the cavity and the shape of the recess rim which most generally can be any function of the two former parameters. However the shape was mostly determined as a function of the length.

[0082] The cavity walls of the recess **2** (see FIG. **6**) offer additional surface which generate additional power that needs to be added to the main power generated by the outer blade wall. It was also observed that the tip leakage flow for a recessed cases blade tip is lower than for a flat tip. The overall mass flow through the computational domain remained unchanged, suggesting that the change in the leakage mass flow occurred prior to the suction side throat region, hence resulting in a constant corrected flow through the rotor. It is important to also note, that variations in total pressure loss coefficients followed those of the tip gap mass flow. The relation between aerodynamic loss and tip leakage mass having been verified, necessitated further reduction of the tip leakage mass flow as an important design criteria. The changes with depth were strongly non-linear, with an optimum depth leading to minimum tip leakage mass flows being identified. This is also an important difference to the tip leakage mass flow evolution in a flat tip case where the tip leakage mass flow varies linearly with the gap height. The changes in recess length were almost linear.

[0083] The understanding of the detailed flow physics is therefore particularly important in the design process and will be investigated next on behalf of three major test cases. The first case is a flat tip blade. The second test case is a nominal recess cavity as known from the prior art with a length of 80% axial chord and twice as deep than the tip gap, the rim thickness being kept constant. This test case represents a current design for recess cavities. The final test case is the newly designed recess geometry based on the extensive physical modelling and geometric perturbation.

[0084] FIG. **3** shows in an exemplary manner a flow field around a common turbine blade **100** with a flat tip **101** with two main flow structures. The first one is the tip passage vortex **102** which forms when incidence driven fluid enters the tip gap from the suction side at leading edge and leaves it again after approx. 20% axial chord. Furthermore tip leakage occurring on the pressure side between leading edge and approx. 15% axial chord crosses the tip gap and mixes with the incidence flow in the tip passage vortex. The feeding of the tip passage vortex is well organized, with the flow past a dividing streamline triggering the formation of the tip passage vortex. The succeeding pressure side leakage flow feeding the tip passage vortex can also be identified.

[0085] The second main flow feature observed is the tip leakage vortex **103** that forms from the tip leakage flow crossing the gap from the pressure side starting at approx. 15% axial chord. The dividing streamline between the pressure side leakage feeding the tip passage vortex and the tip leakage vortex outer fluid layer can be identified. The outer fluid layers in the tip leakage vortex **103** result from the main part of the pressure driven, low gap shear loss generating leakage jet. The tip leakage vortex core is formed by blade tip boundary layer fluid.

[0086] A cutting plane orthogonal to the blade mean camberline reveals the well known gap flow structure. When the tip leakage flow enters the gap from the pressure side, a separation bubble is formed, leading to a vena contracta. The leakage jet leaving the vena contracta would then form the wake fluid in the lower part of the gap. This wake creates mixing loss and is found later in the tip leakage vortex core. The leakage jet above the wake part is often modelled as an isentropic jet, it forms the outer fluid layers around the tip leakage vortex core depending on the axial position when it left the gap on the suction side.

[0087] FIG. **4** schematically shows a flow structure around the turbine blade **51** according to FIG. **2** with the recess **52** at its tip **53**. The recess **52** has in a circumferential and in vertical direction (in the direction of the length of the turbine blade) over most of its length—with exception to the trailing edge **62**—an in general constant wall thickness. It should be noted that the flow structure is dependent on the aerodynamic design of the turbines, varying somewhat for different turbine blade rotor designs and may therefore not exactly match the following descriptions. Despite of this, it is believed that many of the flow features in general remain the same for modern axial high work turbines, with the sensitivities and the trade-studies relating to geometrical variation remaining applicable. It was found that in total six main flow features influencing the cavity flow. Starting at the leading edge **60** of

the pressure side, fluid above the blade leading edge stagnation point **61** fluid of the passage enters the cavity **52**. It crosses the cavity with low loss and at the flow angle of fluid at leading edge, and impinges on the corner between the cavity bottom and cavity suction side wall shortly following the peak suction. After hitting the corner wall this pressure side leading edge jet rolls up into a vortical structure C and moves downstream inside the cavity **52**, partly leaving the cavity **52** and entering the suction passage flow again. The boundary layer on the recess rim entering the cavity along the whole pressure side **20** due to the tip clearance pressure gradient and on the first 20% axial chord on the suction side immediately rolls up into a vortex A in the corner between the cavity bottom and the cavity walls, stretching along the whole pressure side **20** to the end of the cavity and reaching up to 20% of axial chord on the suction side **21** cavity wall. After 10% of the axial chord, this suction side part of the vortex C is lifted off the cavity bottom by an incidence driven suction side leakage jet entering the cavity. A third important flow feature is vortex B which forms when casing boundary layer fluid rolls up against the pressure side tip leakage jet TL. This vortex stays on the casing wall and deflects the pressure tip leakage inside the cavity as shown in FIG. **5**. Between the above two vertical flow structures, a dividing streamline DS1 establishes.

[0088] Downstream of the 20% axial chord, the flow behaviour of the pressure side leakage is similar to the flat tip case with the difference that the leakage is deflected by the cavity vortices and interacts with them. After leaving the gap on the suction side, this fluid forms again the outer layer of the tip passage vortex and the tip leakage vortex. The core of the tip passage vortex is formed by the same incidence tip leakage that lifts off the cavity corner vortex when entering and leaving the cavity between 10% and 20% axial chord. The core of the tip leakage vortex is wake fluid behind the separation bubble on the suction side rim that forms when the pressure side leakage jet leaves the cavity.

[0089] To additionally clarify the flow features inside the cavity a cutting plane orthogonal to the camberline located downstream of the formation of the vortex formed by the pressure side leading edge jet is shown in FIG. **5**. The three main cavity vortices above are referenced. Between the casing vortex B and the rim boundary layer roll up vortex A the pressure side leakage crosses the cavity lifting up vortex C caused by the pressure side leading edge cavity jet. Two separation bubbles form, one at the pressure side rim edge to the outer blade wall when the tip leakage jet enters the gap, and the other on the suction side rim edge with the cavity wall when the tip leakage leaves the cavity again. The tip leakage jet is recognizable as a low entropy zone between the higher entropy zones where the vortices are located. The casing vortex is rather squeezed, this explains why downstream of the blade gradually more and more fluid from the neighbouring vortices mix in.

[0090] The nominal design showed many vortical structures inside the recess cavity. Particularly the front part of the cavity is affected by these structures. As seen above, the boundary layer fluid leaking from the rim into the cavity rolls up in a vortex along the corner between cavity bottom and cavity rim wall. The aim of the new design was to eliminate the recirculation zone in the front part of the blade to minimize aerodynamic losses and reduce the head transfer coefficient.

[0091] FIG. **6** shows a flow distribution around a tip **3** of a of turbine blade **1** according to the present invention. The recess **2** is surrounded by a wall **4** which has in circumferential direction a variable wall thickness t. Whereby the wall **4** has a maximum thickness t on the suction side **21** in the area where the turbine blade **1** has the maximum over all thickness. A side surfaces **5** of the recess **2**, respectively the wall **4**, is here arranged in general parallel to the length axis of the turbine blade **1** (in general perpendicular to an end surface **6** of the turbine blade **1**). However, depending on the field of application, alternative designs may be appropriate. One advantage consists in that the shown design is relatively easy to make by standard grinding processes.

[0092] One effect of the improved design is that the streamline that separates the recirculation zone from the pressure side leading edge jet is moved. In FIG. **6** the effect of the improved design on the cavity flow pattern is shown. The recirculation on the leading edge **10** is suppressed. The pressure side leading edge jet now spreads inside the whole cavity **2**. The casing boundary layer fluid rolls up into vortex B and interacts with the fluid from the pressure side leading edge jet. The fluid trapped in the recirculation in the nominal design now enters the cavity and is pushed out again by the pressure side leading edge jet. After leaving the cavity it feeds the tip passage vortex.

[0093] FIG. **7** illustrates the vortical flow pattern inside the cavity **2** and around the tip **3** of the turbine blade **1** along a cutting plane parallel to the length direction of the turbine blade **1**. As it can be seen the end surface **6** of the turbine blade **1** is delimited by a gap **12** from the casing **8** of the turbine. The vortices A and B are actively interacting. Therefore vortex B is not confined to the casing anymore but can occupy the whole cavity volume. Vortex C is formed by the fluid that led to the suction side leading edge recirculation in the nominal case. It is formed when this fluid separates on the cavity rim while being pushed out of the cavity by the pressure side leading edge jet.

[0094] Subsequent the results regarding aerothermal performance of three test cases are introduced. For the aerodynamic performance, the tip leakage mass flow is investigated since it is intensively related to the total pressure loss. Nusselt Number distribution and integrated heat flux vector on the blade tip walls are compared to assess the impact of the new design on heat transfer.

[0095] FIG. **8** shows the variation of accumulated tip gap mass flow from leading to trailing edge for the pressure and the suction side for the three investigated test cases are shown separately. In the diagram x means length, c_ax the axial cord and mdt* the leakage mass flow over the blade tip as a function of the axial distance. On the pressure side, the most important feature is the growth of the accumulated tip gap mass flow from leading edge to trailing edge for the flat tip compared to a linear increase as long as the recess cavity opens behind the rim. Downstream of the cavity trailing edge the accumulated tip gap mass flow also varies non-linearly and is similar to the flat tip case for in both recess designs. The linear increase may be explained through the average static pressure variation at the tip gap entry on pressure side and its exit on the suction side.

[0096] As shown in FIG. **9**, the static pressure decreases both for the pressure and the suction side non-uniformly in the flat tip case. The diagram shows the static pressure variation as a function of the axial length. For the recess cases however static pressure remains at constant level whenever tip leakage

enters the cavity, which is the case for the entire pressure side gap but also for the front part of the suction side, where incidence fluid enters into the cavity. The recess cavity acts like a reservoir where pressure remains constant. The sealing effect and the resulting reduction of the accumulated tip gap mass flow is clearly observed. The nominal recess case showed a reduction of 23% in the leakage mass flow when compared to the flat tip, the new design had 25% less mass flow crossing the gap compared to the flat tip.

[0097] FIG. **10** shows the accumulated tip clearance mass flow on the gap exit for the blade suction side is shown for a flat tip blade (prior art), the a recess with a constant wall thickness (nominal recess, prior art) and an improved recess with variable wall thickness (indicated as new design, according to the present invention). The incidence driven tip leakage mass flow is much more intense in the recess cases than in the flat tip case. Incidence leakage reaches for all three cases from leading until 22% axial chord. However the amount of mass flow entering the recess cavities is almost the double of the one for the flat tip. This sustains again the cavity in acting as a reservoir to be filled up with fluid. The difference in the amount of mass flow additionally having entered the cavity compared to the flat tip gap almost exactly matches with the reduction in total cumulated tip leakage mass flow over the entire suction side. No large differences in tip gap mass flow are noted between the nominal and the new recess designs.

[0098] FIG. **11** shows the heat transfer at the tip of three different turbine blades. While FIG. **11***a* shows in a comparative manner the Nusselt Number (Nu Number) distribution of a common turbine blade with a flat end surface as shown in FIG. **3**, FIG. **11***b* and **11***c* show the distribution at turbine blades with recesses according to the prior art (indicated as "nominal") and the present invention (indicated as "new"). High Nusselt Numbers occur on the leading edges in all three cases. This is where hot fluid meets the blade tip first and heat transfer is highest. On the pressure side edges Nusselt Number has the same magnitude in all three cases. The thin rim of the nominal recess shows a similar distribution on the suction side front part compared to the new design. When the tip leakage vortex at forms (about 25% axial chord), the value of the Nusselt Number drops for both the flat tip case and the nominal recess case. This observation can however not be made for the suction side rim of the new design. Both the flat tip and the nominal recess show high Nu Numbers at the leading edge. In the new design however, Nu Number values do not reach as high on the cavity bottom. From FIG. **11** the differences between the improved design with a recess according to the present invention (indicated as "new") and a flat tip (indicated as "flat") is visualized. The blocking of the suction side recirculation zone by a thicker rim has not lead to higher Nusselt Numbers on the rim.

[0099] FIG. **12** visualizes the heat load of different turbine blades. The integrated heat flux vector on the blade tip of a common flat blade tip (indicated as "flat") and a blade tip with a recess according to prior art (indicated as "nominal") and the present invention (indicated as "new") gives the heat load for the three test cases.

[0100] From FIG. **12** where heat load is split according to the affected wall type the following observation can be made. The overall predicted tip heat load is highest for the flat tip and lowest for the improved design with a variable wall thickness ("new" design). The reduction of heat load between the flat tip and the new design (about 14%) is about twice as high than between the nominal and the new recess design (70%). However it must be noted, that the new design also has higher regions of heat load than the nominal design. This is the case for the tip rim and the cavity walls to which the cavity rim walls and the remaining rear flat blade tip portion belongs. Increasing the rim thickness, as well as a deeper and shorter cavity are the reasons for this increased heat load. However it has also been shown that changing the flow field on the leading edge inside the cavity through the elimination of the suction side recirculation zone has proved effective in reducing heat load on the cavity bottom.

[0101] In the FIGS. **13** and **14** the computed results from CFD predictions (see FIGS. **3-12**) are compared to experimental results which have been performed in a confidential manner at the Swiss Federal Institute of Technology (ETHZ). The flat tip and the new recess design blades have been experimentally evaluated at ETHZ axial turbine facility LISA.

[0102] FIG. **13***a* shows the experimental relative total pressure coefficient distribution at 14% axial chord downstream rotor blade trailing edge for flat tip blade. First the predicted and experimental relative total pressure loss coefficients for the flat tip and the new recess design are compared in 2D axial cutting planes located 14% axial chord downstream of the rotor trailing edge. The experimental data for the flat tip blade shown in FIG. **13***a* are snapshots at a given point in time of an unsteady flow. Therefore unsteady flow features are resolved which are not present in the single row steady state CFD results. The fact of unsteady data also explains the modulation of the low relative total pressure zones identifying the secondary flow vortices and the tip leakage vortex.

[0103] FIG. **13***b* shows the CFD predictions from a single row steady state computation. The computationally predicted relative total pressure loss coefficient resolves in sufficiently good accuracy the secondary flow structures measured by the experiment. The hub and tip passage vortex are captured both in their spatial extension and in the loss magnitude. Also the trailing edge wake of the rotor blade is captured in the CFD results. The loss region associated to the tip clearance vortex is however over predicted compared to the experiment. As was mentioned above

[0104] FIG. **13***c* shows CFD predicted and measured pitch averaged radial distributions of relative flow yaw angle at 14% of the axial chord downstream of the rotor blade trailing edge for the flat tip blade. It can be seen that the variation in the relative yaw angle due to the tip leakage vortex between 80% span and 100% span is largely over-predicted by the computational result. The magnitude of relative yaw angle variation due to the hub and tip secondary flow structure is well predicted.

[0105] FIGS. **14***a* and **14***b* show experimental and CFD predicted data for the turbine blade with an improved recess according to the present invention (indicated as "new" design) with a variable wall thickness in circumferential direction are compared. The experimental data shown in FIG. **14***a* are again a snapshot of unsteady data. The snapshots for the flat blade tip and the new recess design were both taken at the same point in time. The CFD predicted relative total pressure coefficient from steady state computations are shown in FIG. **14***b*. It can again be seen that the predicted CFD results resolve the same features that are also captured by the measured flow field. Predicted relative total pressure loss coefficients showing the hub and tip passage vortices agree well with the experimental data. The over prediction of the tip leakage vortex noted in the flat tip case is also found in

the new recess design case. Compared to the computationally predicted relative total pressure loss coefficient for the flat tip case, it can be noted that the spatial extension of the tip leakage vortex loss core for the new recess design has been reduced.

[0106] FIG. **14***c* shows the measured and predicted pitch averaged relative flow yaw angle distributions for the new design. The CFD predicted relative flow angle distribution matches the experimental data up to about 80% of the span. The part from 80% span to 100% span is influenced by the tip leakage vortex. Whereas the secondary flow features on hub and tip are correctly predicted, the difference in flow angle due to the tip leakage vortex is very much over predicted.

[0107] In FIG. **15** the experimentally measured relative yaw angle distributions for the flat tip and the new recess design are presented for the tip region from 60% span to the casing at 100% span. It can be seen that the new recess design shows less over turning than the flat tip blade. This result clearly illustrates that the recess cavity influences the tip leakage vortex which is responsible for the stated overturning.

[0108] Experimentally measured performance data shows that for the turbine used the "new" recess design has a 0.3% total efficiency when compared to the flat tip at exactly the same overall turbine operating conditions. The predicted difference between both efficiencies was 0.38%, which is a good quantitative agreement with the experimental data.

[0109] The predicted heat transfer data is qualitatively compared to data presented by the Ohio State University Gas Turbine Laboratory [12]. A turbine blade with a recess cavity similar to the nominal design presented here was equipped with heat transfer gauges to measure heat transfer on the cavity bottom near leading edge, trailing edge and in the middle. Also the rim was equipped with several gauges. Nusselt Numbers were reported for different vane/blade spacings. The trend in the variation of Nu Number according to the investigated location is similar. The highest Nu Number is found in the leading edge region. The second heat flux gauge was positioned 12.5% blade axial chord from peak suction downstream, reporting almost half of the Nu Number at leading edge. This can also be observed in the nominal recess case from FIG. **11**. Finally the third heat gauge at 62% blade axial chord corresponding to 80% cavity axial chord reports almost the same Nu Number for all vane spacings that was reported for the low vane spacing on the previous one for the short spacing.

[0110] FIGS. **16** and **17** are showing the distribution of the wall thickness in circumferential direction of several recesses of turbine blades according to the present invention. Such that it becomes possible to compare different shapes of recesses of turbine blades, the graphs are shown in a normalized manner in that on the y-axis the thickness t is shown in relation to a reference thickness t**0**. With reference to FIG. **6**, the local thickness t of the wall **4** is measured at the level of the end surface **6** of the turbine blade **1** along and perpendicular to an outer edge **13** of the turbine blade **1**, which is formed by the side surface **7** of the turbine blade **1** and its end surface **6**. The local wall thickness t is shown in the graph on the x-axis starting from the blade leading edge stagnation point 0 (0% circumferential length) in both circumferential directions, whereby the relative position of the trailing edge **11** of the turbine blade **1** is indicated by the values 1 (100%), respectively −1 (−100%). The suction side is positive (+) and the pressure side of the profile is negative (−). The trailing edge **11**, which is in the graph located approximately in the ranges between +0.6 (+60%) and +1 (+100%) and −0.6 (−60%) and −1 (−100%), is not considered in the diagram because of the reducing thickness of the turbine blade in this area. It can be seen that the wall thickness t increases on the suction side and has a (local) maximum 15 on the suction side of the turbine blade, depending on the field of application, in the range between +0.1 (+10%) and +0.4 (+40%) relative length. In other embodiments the maximum 15 is arranged at +11%, 19%, 30%, respectively 37% (aberration +/−5%). The maximum 15 is in certain embodiments arranged in the area of the maximum thickness **14** of the turbine blade. As it can be retrieved from the shown graphs, certain embodiments have a shoulder **16** in the range +0.05 (+5%) and +0.15 (+15%), with a locally reduced augmentation of the thickness (e.g. see FIG. **6**). In an embodiment, the augmentation of the wall thickness (indicated by arrow **17**) already starts on the pressure side of the turbine blade, e.g. in the range between −0.1 and 0. As it can be seen in the graphs, in certain embodiments the increase and the decrease of the wall thickness are in general similar to each other and in the range of 300% to 400% per 0.1 normalized circumferential length. As it can further be retrieved from the graphs, the maximum wall thickness is about 5.5 to 6.5 times thicker than the minimum wall thickness at the pressure side.

[0111] On the pressure side the wall thickness is in certain embodiments constant which is indicated by the in general horizontal progression of the graph in this area. However, certain embodiments (see profile 3) may also have a local maximum 18 at the pressure side.

[0112] Although the present invention has been described in relation to particular embodiments thereof, many other variations and modifications and other uses will become apparent to those skilled in the art. It is preferred, therefore, that the present invention be limited not by the specific disclosure herein, but only by the appended claims.

1. A turbine blade (**1**) comprising:
a side surface (**7**) having an aerodynamic profile and an end surface (**6**) arranged in a mounted position in a turbine delimited by a gap (**12**) from a casing (**8**) of the turbine, the end surface (**6**) comprising a recess (**2**) which is shaped such that it acts as an aerodynamic seal, wherein the recess (**2**) is delimited by a side wall (**4**) which has a variable wall thickness (t) in a circumferential direction of the turbine blade (**1**).

2. The turbine blade (**1**) according to claim **1**, wherein the side wall (**4**) has a generally constant wall thickness (t) in a height direction (**0**).

3. The turbine blade (**1**) according to claim **1** wherein the wall thickness (t) of the side wall (**4**) has an overall maximum (**15**) on a suction side of the turbine blade (**1**) in an area where the turbine blade (**1**) has its maximum thickness (**14**).

4. The turbine blade (**1**) according to claim **1** wherein the wall thickness (t) of the side wall (**4**) has a maximum (**15**) on a suction side of the turbine blade (**1**) between +0% and +50% relative length with respect to the blade leading edge (**0**).

5. The turbine blade (**1**) according to claim **4**, wherein the maximum (**15**) is arranged between +10% and +40% relative length with respect to the blade leading edge (**0**).

6. The turbine blade (**1**) according to claim **4** wherein the maximum (**15**) is an overall maximum.

7. The turbine blade (**1**) according to claim **4** wherein the wall thickness (t) is on the suction side of the turbine blade (**1**) on both side of the maximum (**15**) continuously decreasing.

8. The turbine blade (**1**) according to claim **1** wherein a wall thickness (t) of the side wall (**4**) has on the pressure side of the turbine blade (**1**) a minima in the range between −0% and −70% relative length with respect to the blade leading edge (**0**).

9. The turbine blade (**1**) according to claim **8** wherein the wall thickness (t) on the suction side of the turbine blade (**1**) is at least partially constant.

10. The turbine blade (**1**) according to claim **8** wherein the wall thickness (t) on the pressure side of the turbine blade (**1**) is at least partially constant.

11. The turbine blade (**1**) according to claim **10**, wherein the wall thickness (t) on the pressure side is constant in the range between −5% and −50% relative length with respect to the blade leading edge (**0**).

12. The turbine blade (**1**) according to claim **1** wherein an overall maximum (**15**) of the wall thickness (t) of the side wall (**4**) is about 2 to 8 times bigger then an overall minima.

13. The turbine blade (**1**) according to claim **12**, wherein the overall maximum (**15**) of the wall thickness (t) of the side wall (**4**) is about 5.5 to 6.5 times bigger then the overall minima.

14. The turbine blade (**1**) according to claim **1** wherein the recess (**2**) has a generally constant depth (**0**).

15. A turbine formed with the turbine blade (**1**) of claim **1**.

* * * * *